Solar and Stellar Multi-scale Activity
Proceedings IAU Symposium No. 400, 2026
S. Vargas-Domínguez & J. C. Buitrago-Casas, eds.
doi:10.1017/S1743921326107182

Numerical study of oscillations in prominence threads generated by plasma flow

Sofya Belov[1], Robert Erdélyi[2,3,4] and Petr Jelínek[1]

[1]University of South Bohemia in České Budějovice, Faculty of Science, Department of Physics
email: belovs00@prf.jcu.cz

[2]University of Sheffield, School of Mathematics and Statistics, Solar Physics and Space Plasma Research Centre (SP2RC)

[3]Eötvös Loránd University, Department of Astronomy

[4]Hungarian Solar Physics Foundation (HSPF), Gyula Bay Zoltan Solar Observatory (GSO)

Abstract. We study transverse (kink mode) oscillations in the threads of solar prominences. These structures can exhibit both individual and collective behavior when groups of threads oscillate with their own periods, independent of the rest of the prominence. Several studies have suggested that these and some other oscillatory phenomena in the solar atmosphere may be explained by the phenomenon of vortex shedding, which has been widely studied in hydrodynamics but has not yet been satisfactorily investigated under magnetohydrodynamic conditions, such as those present in the solar atmosphere. We study prominence oscillations in association with vortex shedding numerically using the magnetohydrodynamic approach in three dimensions. We model the structures as groups of flexible cylindrical bodies, which allows us to study both their collective and individual behaviors. Specifically, we ran a simulation with a group of three vertically aligned cylindrical bodies and three simulations with two horizontally aligned cylindrical bodies at varying distances to evaluate the influence of separation distance.

Keywords. vortex shedding, coronal mass ejection, kink oscillations, solar prominences

1. Introduction

Wave and oscillatory phenomena are omnipresent throughout the entire solar atmosphere. They are the subject of theoretical and observational studies related to the unsolved problem of heating the solar corona and the acceleration of the solar wind. The oscillations are interpreted in terms of magnetohydrodynamic (MHD) waves.

There exist many modes of oscillations, where transverse (kink) oscillations are one of the most studied wave phenomena in the solar atmosphere (Aschwanden 2005; Priest 2014; Nakariakov *et al.* 2021). They have been observed in coronal loops, solar prominences, or flux ropes, which are often defined as clusters of magnetic field lines twisting around a common axis.

Nakariakov *et al.* (2009) present a model suggesting that a possible mechanism for the excitation of kink oscillations is coronal mass ejections (CME) causing the vortex shedding phenomenon. This phenomenon, which is well known and described in hydrodynamic conditions, consists of a periodic alternate formation of vortices from each of the two sides of a blunt flow obstacle, which can form a structured chain of vortices called the Kármán vortex street. The frequency of the process depends on the obstacle

© The Author(s), 2026. Published by Cambridge University Press on behalf of The International Astronomical Union.

https://doi.org/10.1017/S1743921326107182 Published online by Cambridge University Press

size and fluid velocity according to the Strouhal number (Strouhal 1878). In the model mentioned above, the blunt obstacle is represented by the upper horizontal section of a magnetic structure surrounded by vertical flow originating from a CME. The numerical study in Jelínek *et al.* (2022) suggests that vortex shedding might excite kink oscillations in prominence threads.

2. Model and method

This study follows from our study presented in Jelínek *et al.* (2022). This included a parametric study of vortex shedding around a single motionless cylinder with five different initial magnetic field values and a study of the oscillations of a single flexible cylinder excited by vortex shedding. For the calculations, we use the `LARE3D` code, which is a well-tested, parallel, and open science simulation code. `LARE3D` is a Lagrangian-Eulerian remap numerical code that implements a staggered grid and is second-order accurate in space and time (Arber *et al.* 2001). The code uses the Lagrangian-remap method, splitting each time step into a Lagrangian step followed by a remap step, which does not involve adapting the grid resolution. When the medium is deformed, the grid evolves according to the fluid flow that caused this deformation. After that, the grid is remapped to its original state by Van Leer gradient limiters, which, apart from the interpolation inaccuracies, do not affect the fluid variables and only transfer them to the cells of the remapped grid – see, e.g., Griffies *et al.* (2020).

2.1. *Governing Equations*

In our numerical model, the plasma dynamics is described by the 3D, time-dependent ideal MHD equations in the Cartesian coordinate system, which can be written in the following form – e.g. Arber *et al.* (2001):

$$\frac{\mathrm{D}\,\rho}{\mathrm{D}\,t} = -\rho\nabla\cdot\mathbf{v}, \tag{1}$$

$$\rho\frac{\mathrm{D}\,\mathbf{v}}{\mathrm{D}\,t} = -\nabla p + \mathbf{j}\times\mathbf{B}, \tag{2}$$

$$\frac{\mathrm{D}\,\mathbf{B}}{\mathrm{D}\,t} = (\mathbf{B}\cdot\nabla)\mathbf{v}, \tag{3}$$

$$\frac{\mathrm{D}\,e}{\mathrm{D}\,t} = -\frac{p}{\rho}\nabla\cdot\mathbf{v}, \tag{4}$$

$$\nabla\cdot\mathbf{B} = 0, \tag{5}$$

where all the terms have their usual meanings. As follows from Eq. 2, gravitational acceleration is not considered in the model. Also, fully ionized plasma was considered (and therefore the adiabatic coefficient was set as $\gamma = \frac{5}{3}$) with an average mass of ions $1.2m_{\mathrm{p}}$, typical for the solar corona.

2.2. *Initial State*

Figure 1 illustrates the simulation boxes in the initial state of each of the two studied cases (the one used for case #1 was covered by $360\times360\times1200$ grid points, i.e. its spatial resolution was 0.0167 Mm approximately; the one used for case #2 was covered by $444\times1110\times999$ grid points, i.e. its spatial resolution was 0.009 Mm approximately). The parameters set in the initial conditions of each simulation are summarized in Tab. 1. All initial parameters are set in accordance with the equilibrium condition.

https://doi.org/10.1017/S1743921326107182 Published online by Cambridge University Press

Table 1. Initial parameters of the studied cases.

	Case #1	**Case #2**
v_{z0}	$1.784 \cdot 10^5\,\mathrm{m\,s^{-1}}$	$8.921 \cdot 10^4\,\mathrm{m\,s^{-1}}$
B_e	10^{-3} T	10^{-3} T
B_i	$1.029 \cdot 10^{-3}$ T	$1.032 \cdot 10^{-3}$ T
ρ_e	$10^{-12}\,\mathrm{kg\,m^{-3}}$	$10^{-12}\,\mathrm{kg\,m^{-3}}$
ρ_i	$5 \cdot 10^{-11}\,\mathrm{kg\,m^{-3}}$	$10^{-11}\,\mathrm{kg\,m^{-3}}$
T_e	$2 \cdot 10^6$ K	$2 \cdot 10^6$ K
T_i	$6 \cdot 10^3$ K	10^4 K
βe	0.069	0.069
β_i	0.010	0.003

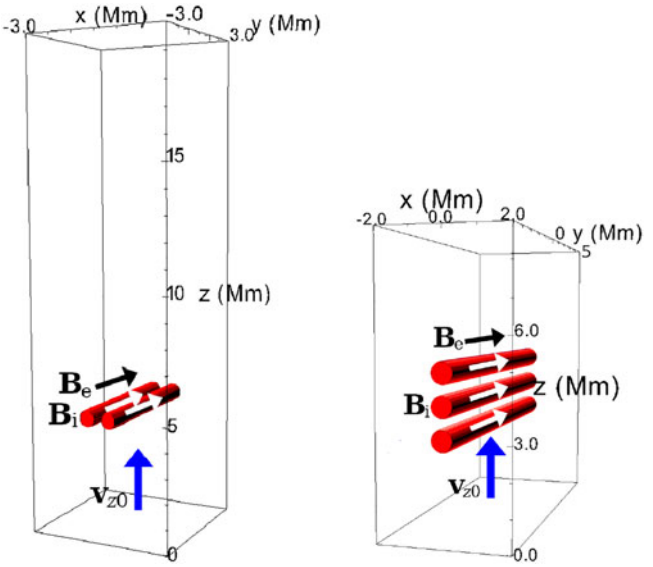


Figure 1. The sketches of the numerical boxes (not to scale) for cases #1 (left) and #2 (right) including their sizes. The red cylinders represent the obstacles. The initial flow is denoted as $\mathbf{v}_{z0}$.

We consider two model cases: #1 – with two flexible cylindrical obstacles located next to each other with a radius square $r^2 = 0.1\,\mathrm{Mm}^2$, fixed at the boundaries, with only the y component of the magnetic field applied, with the centres $2r$, $3r$ and $6r$ apart; and #2 – with the same configuration, except there are three obstacles located above each other with the centres $3r$ apart. There is a flow coming from the lower face of the box constantly throughout the simulations.

3. Numerical Results

3.1. *Flow and oscillations*

Figures 2 to 3 show the distribution of the mass density in the plane $y = 0$ of cases #1 and #2. The panels are shown for different time steps.

In case #1, all three simulations show initial decaying oscillations in the xz plane and deformations before stabilizing (see movies linked via QR codes). In the $2r$ configuration (cylinders in contact), vortex shedding appears later ($t \approx 730$ s), leading to a single Kármán vortex street and kink mode oscillations. In the $3r$ configuration, vortex shedding occurs earlier but does not trigger oscillations; instead, two opposing Kármán vortex street halves form due to the destructive interference of the vortices in the centre. The

https://doi.org/10.1017/S1743921326107182 Published online by Cambridge University Press

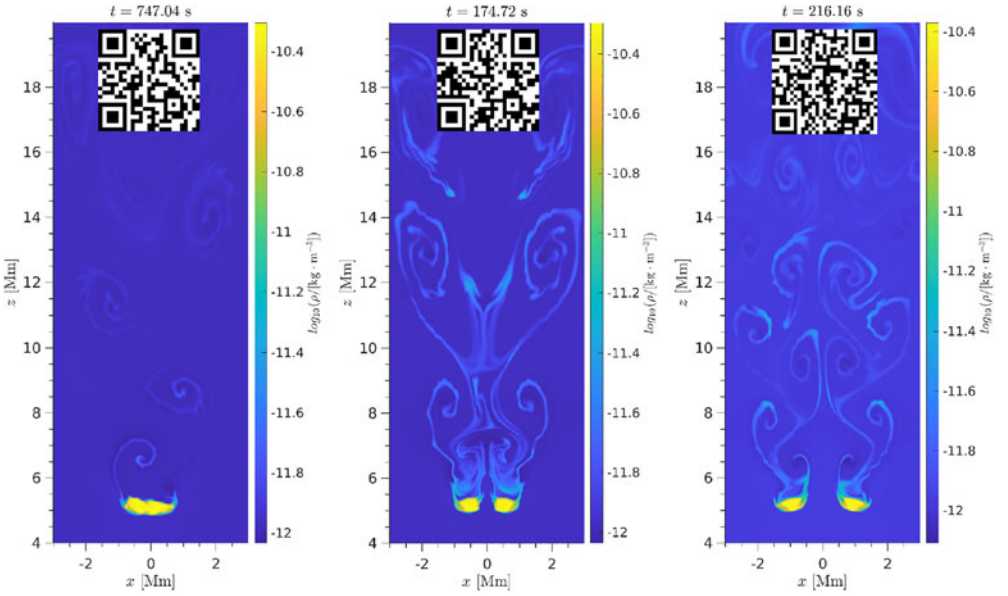


Figure 2. Mass density distribution in case #1 at configurations $2r$, $3r$ and $6r$ respectively at different time steps indicated above. In each case, vortex shedding is taking place - see movies at QR codes. $2r$: Kármán vortex street is captured; $3r$: two halves of Kármán vortex streets are captured; 6r: two opposite Kármán vortex streets are captured.

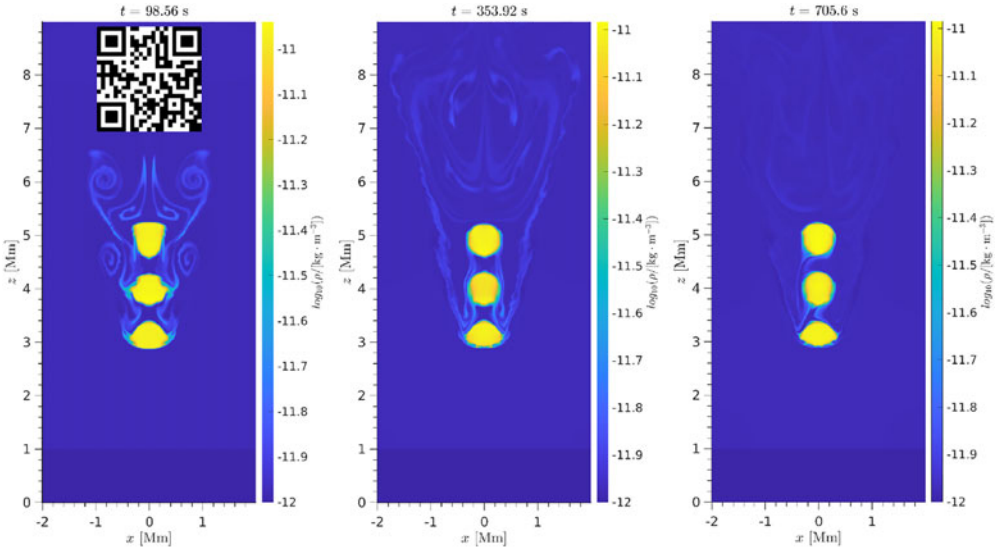


Figure 3. Mass density distribution in case #2 at different time steps indicated above.

$6r$ case also shows early vortex shedding, forming two Kármán vortex streets without triggering oscillations.

In case #2, clear vertical oscillations of magnetic structures are observed in the beginning. Also, a symmetric pair of vortices forms, but the symmetry does not break, and vortex shedding does not take place.

https://doi.org/10.1017/S1743921326107182 Published online by Cambridge University Press

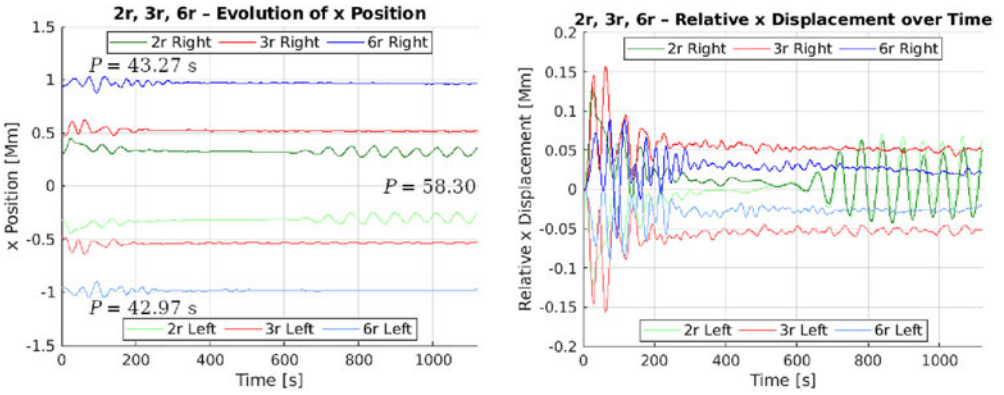


Figure 4. Left: evolution of absolute x-position; right: evolution of relative x displacement i.e. x displacement from initial positions, for two cylinders with the centres initially separated by $2r$, $3r$ and $6r$ (case #1), period values calculated by wavelet analysis (Torrence & Compo 1998) are indicated.

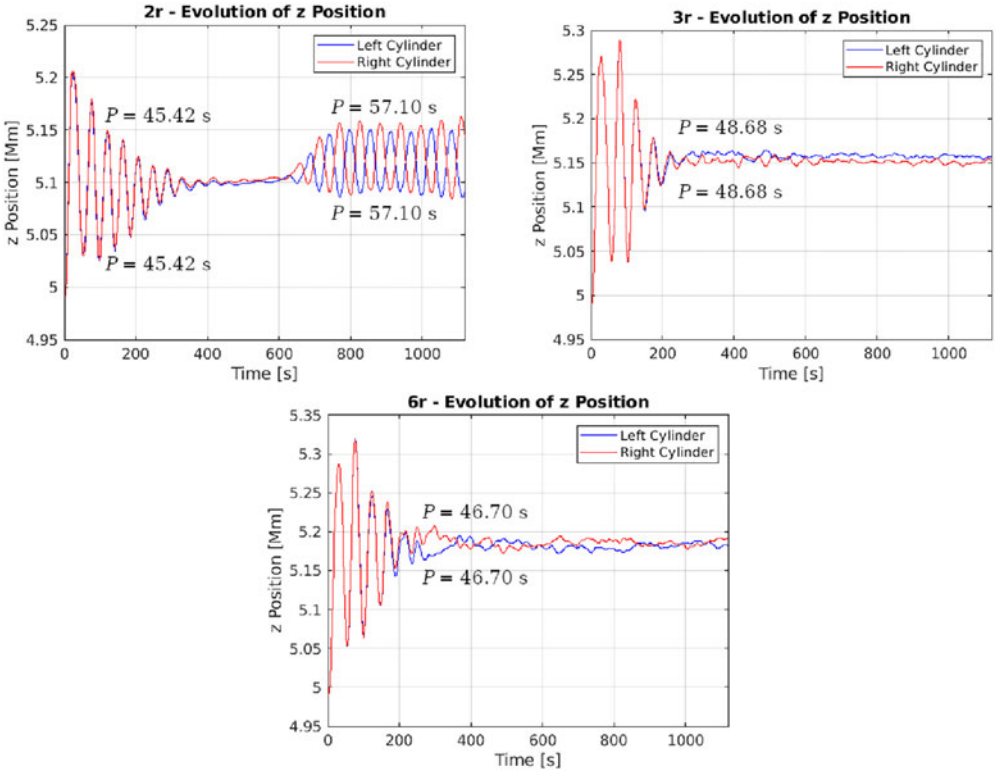


Figure 5. Evolution of absolute z-position for two cylinders with the centres initially separated by $2r$, $3r$ and $6r$ (case #1), period values calculated by wavelet analysis (Torrence & Compo 1998).

3.2. *Oscillation analysis*

In Figs. 4–6, we approximately recorded the motion of the cylinders in the xz plane by locating the geometrical centre of the area identified as the cylinder's transverse cross-section using the threshold method. In all #1 cases, the cylinders begin with decaying

https://doi.org/10.1017/S1743921326107182 Published online by Cambridge University Press

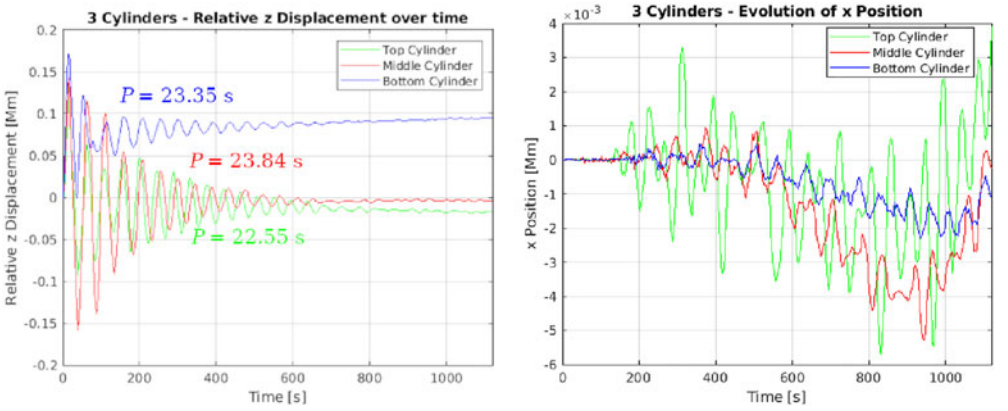


Figure 6. Left: evolution of relative z displacement i.e. z displacement from initial positions; right: evolution of absolute x-position, for three cylinders with the centres initially separated by $3r$ (case #2), period values calculated by wavelet analysis (Torrence & Compo 1998).

oscillations in the xz plane. The motions are slightly different but roughly symmetric within each pair. As shown in Fig. 5, z-direction oscillations are the strongest in case $3r$; in the beginning, case $2r$ shows slightly more frequent z oscillations. Regarding the x motion (Fig. 4), the cylinder centres stabilize at a further x distance from each other compared to the initial distance; surprisingly, in the $3r$ configuration, the cylinders end up in the furthest position relative to the initial one; the $6r$ configuration leads to the most numerous oscillations in the x-direction. In case #2, a phase shift is observed between the middle and top cylinders, where the top one is ahead of the middle one (Fig. 6).

4. Conclusions

Overall, initial oscillations in the xz plane occur in all configurations of the case of plasma flow around two magnetic structures located side by side. Initial z oscillations occur in the case of plasma flow around three magnetic structures located above each other. Vortex shedding can lead to kink mode oscillations, but it does not always trigger them. The spatial configuration influences the amplitude, frequency and duration of the resulting motions.

Acknowledgements

The work in this article is part of the project DynaSun. This project DynaSun has received funding under the Horizon Europe programme of the European Union under grant agreement (no. 101131534). Views and opinions expressed are, however those of the author(s) only and do not necessarily reflect those of the European Union and therefore, the European Union cannot be held responsible for them. This work was supported by the Ministry of Education, Youth and Sports of the Czech Republic through the e-INFRA CZ (ID:90254).

References

Arber, T. D., Longbottom, A. W., Gerrard, C. L., Milne, A. M. 2001, *JCoPh*, 171, 151

Aschwanden, M. J. 2005, *Physics of the Solar Corona. An Introduction with Problems and Solutions* (2nd; New York: Springer)

Griffies, S. M., Adcroft, A., Hallberg, R. W. 2020, *JAMES*, 12, e01954

Jelínek, P., Belov, S., Karlický, M. 2022, *ApJ*, 941, 124

https://doi.org/10.1017/S1743921326107182 Published online by Cambridge University Press

Nakariakov, V. M., Aschwanden, M. J., Van Doorsselaere, T. 2009, *A&A*, 502, 661
Nakariakov, V. M., Anfinogentov, S. A., Antolin, P. *et al.* 2021, *SSRv*, 217, 73
Priest, E. 2014, *Magnetohydrodynamics of the Sun* (Cambridge: Cambridge Univ. Press)
Strouhal, V. 1878, *AnP*, 241, 216
Torrence, C., Compo, G. P. 1998, *BAMS*, 79, 61

https://doi.org/10.1017/S1743921326107182 Published online by Cambridge University Press